JOURNAL OF PROPULSION AND POWER
Vol. 17, No. 3, May–June 2001

Computational Optimization of a Hypersonic Rectangular-to-Circular Inlet

John W. Sabean* and Mark J. Lewis†
University of Maryland, College Park, Maryland 20742-3015

A numerical optimization process utilizing a computational flow solver is applied to the design of a three-dimensional hypersonic inlet. A stream-traced power law compression surface is designed to utilize nonuniform flow at a rectangular capture cross section and transform it to uniform flow at a cylindrical combustor. The objective is to utilize an inversely designed compression forebody with a complex three-dimensional inlet without sacrificing flow uniformity at the combustor plane. A computational flow solver is used to solve the inviscid three-dimensional Euler equations. The standard deviation in pressure across the combustor plane is then calculated. This value serves as the objective function that is minimized in a numerical optimization program. The results show that the area-averaged standard deviation in pressure across the combustor plane can be reduced to as low as 9.9% from an initial value of 16.9%. It is also shown that the three-dimensional geometry can be used to weaken or cancel the main compression shock. As a result, the best transition from rectangle to circle for uniform flow is not monotonic. The inviscid performance of this three-dimensional inlet is then compared to a rectangular-to-circular transition inlet with uniform capture properties, as well as to a simple two-dimensional inlet.

Nomenclature

A_i	=	area of grid face i
i, j, k	=	computational grid directions
M	=	Mach number
P_i	=	pressure at grid cell i
R	=	radial distance from combustor centerline to transition wall
X_n, Y_n	=	nth Bezier–Berstein control point
γ	=	ratio of specific heats
Δ	=	percentage value to determine hyperelliptic and circular average
η_c	=	adiabatic compression efficiency
η_{ke}	=	kinetic energy efficiency
π_c	=	total pressure recovery

Subscripts

cap	=	capture plane property
com	=	combustor plane property
fore	=	ratio over inlet forebody
trans	=	ratio over inlet transition piece
l, x	=	lower inlet transition quadrant
u, x	=	upper inlet transition quadrant
∞	=	freestream property

Introduction

THE design of an efficient compression system for an airframe-integrated scramjet engine is essential for acceptable performance of a hypersonic airbreathing vehicle. The geometry of such hypersonic inlets has normally been restricted to two-dimensional configurations to simplify the analysis and reduce boundary-layer losses. However, there are advantages to exploring the design of inlets that are three-dimensional in nature. One example of this is the combination of a rectangular capture area with a cylindrical combustor, which provides several appealing benefits.

A cylindrical combustor offers several performance benefits over a rectangular cross section. Besides the reduced structural mass required to contain a specific pressure, the cylindrical design reduces the deleterious viscous effects inside the combustor. The problem of hypersonic corner flow is reduced by the elimination of the corners in the transition duct. The hydraulic diameter of the cylindrical combustor cross section is also 20% less than its two-dimensional counterpart, thus reducing the viscous drag inside the combustor by approximately the same proportional amount. This can lead to a substantial overall drag reduction, depending on the length of the combustor.

One problem with the use of a cylindrical combustor is matching it to a rectangular inlet capture area. There is a strong desire for inlets to be stackable when designing a realistic vehicle configuration. Rectangular inlets are of interest because they can be stacked in such a configuration without leakage; stacking circular capture areas would result in mass flow being lost between adjacent inlets. Another consideration is that in many vehicle designs, long flat surfaces are used for forebody compression to delay boundary-layer transition. In addition, the planar shocks associated with a circular capture area would also result in less efficient mass capture. The design of a rectangular-to-circular transition duct, with minimal losses, would provide for an ideal combination of these two efficient, yet very different geometries.

The design of such a transition has recently been studied by Smart,[1] who uses a stream-tracing method to determine the shape of various transitions. The design process involves the use of an axisymmetric compression surface with the flowfield calculated numerically. Different capture area cross-sections are prescribed, varying from rectangular to elliptical in shape. Streamlines are then traced through the flowfield to determine the corresponding inlet wall and exit plane geometries. Circular and elliptical exit planes are then prescribed, with streamlines traced backward through the flow, to determine the corresponding capture plane geometries. The shapes are blended together with a mathematical lofting procedure to produce a smooth transition from rectangle to ellipse. The results of the design of this rectangular-to-elliptical shape transition (REST) have shown that these types of inlets can perform more efficiently than their two-dimensional counterparts.[1]

A numerical optimization can provide insight into the important aspects of a given inlet geometry. The design of a two-dimensional inlet using numerical optimization and a computational code was accomplished by Shukla et al.[2] This study showed that, given adequate control over the inlet geometry, a numerical optimizer coupled

Received 7 October 1999; revision received 11 September 2000; accepted for publication 20 October 2000.

*Graduate Research Assistant, Department of Aerospace Engineering. Student Member AIAA.

†Professor, Department of Aerospace Engineering. Associate Fellow AIAA.

with a computational code can significantly reduce the strength of the reflected shock and provide more uniform flow to the combustor.

It is appealing to consider the idea of a three-dimensional inlet transition duct capable of producing uniform outflow from a nonuniform inflow. Such a geometry would be of particular use when matched to inversely designed forebodies. These inverse-design shapes, including the so-called waveriders, offer benefits to overall vehicle performance, such as a high lift-to-drag ratio.[3] The design of these shapes involves the use of a known flowfield produced by a chosen generating body. The shape of the forebody is then determined by selecting a stream surface in this flowfield that intersects the generated shock wave. Inversely-derived forebodies generated from conical or power-law flowfields will deliver nonuniform flow to the inlet plane, though with known properties. One of the goals of the present work is to optimize a transition duct, which can make the flowfield more uniform before it enters the combustor.

The present work provides a method of directly optimizing the geometry of a rectangular-to-circular transition. Two optimizations are accomplished: a configuration with uniform flow entering the transition duct and a configuration with an inversely derived power-law flowfield inflow. The objective for each optimization is to produce an inlet with uniform pressure at the combustor, for a Hyper-X class[4] aircraft configuration designed for Mach 10 cruise, although other objectives could be chosen. A computational code is used to compute the flowfield produced by a given three-dimensional geometry. This code is then called iteratively by an optimizer to minimize the standard deviation in pressure across the combustor area, to determine a geometry that will produce uniform pressure. For the uniform inflow case, the inflow conditions to the flow solver are set to be the conditions produced by a series of three, two-dimensional flat ramps. For the nonuniform case, a computational code is used to compute a power-law flowfield outside of the optimizer. Streamlines are then traced through this flowfield to determine the properties at the capture plane of the inlet. This method can be extended to optimize the geometry for various figures of merit, and the requirement for uniform pressure can be added as a constraint to the optimizer. Various geometric parameters are studied, and the most significant parameters are chosen to be used with the optimizer. Both geometries are then compared to a two-dimensional inlet operating at the same design conditions.

Numerical Tools

For both of the optimizations presented in the present work, two commercially available numerical tools were utilized.

Inlet Flowfield Computations

The computations of the flowfield inside the inlet were performed using GASP.[5] This code is used to solve the three-dimensional Euler equations. Because of the swept surfaces that appear inside the inlet with impinging shocks, the possibility of separation of a turbulent boundary layer exists; however, for purposes of simplifying the optimization, inviscid flow is assumed. Future work will incorporate Korkegi's[6] separation correlation directly into the optimization as a constraint.

The flowfield is supersonic at all points in the calculation, and, as such, space marching can be used to decrease the total amount of CPU time required to obtain a solution. The full flux is used in the marching direction k with catastrophic limiting of the mixture density and pressure, in which a first-order interpolation is used if either of these values becomes negative for a particular cell face. In the axial directions, i and j, GASP is set to use Roe's flux-difference splitting and a min–mod limiter. The time integration is done implicitly using a two-factor approximate factorization on a single plane, for a constant value of k, with relaxation in the sweep direction. All calculations were made using nonreacting air with a constant ratio of specific heats, $\gamma = 1.4$.

The grid used to calculate the inlet flowfield was $60 \times 40 \times 135$ in size. The grid was then extended 31 points in the marching direction to allow for enough additional planes to calculate the objective function properly. The properties at the inflow plane of the solution were set corresponding to those appropriate for forebody used for the given optimization case. The entire computation of the objective function required approximately 36 min of CPU time on a DEC Alpha 433.

Optimization Method

The optimization was performed utilizing the DOT software package, by VMA Engineering.[7] The software was set to use the Broyden–Fletcher–Goldfarb–Shanno (BFGS) search direction algorithm, which is a quasi-Newton method that finds the search direction by approximating the inverse of the Hessian matrix. The BFGS algorithm is chosen because of its fast convergence. The gradients used in the algorithm were calculated using finite differences. For purposes of this study, no constraints were imposed on the optimization.

Uniform Inflow Optimization

The goal of this optimization is to design a rectangular-to-circular transition, and, as such, several portions of the vehicle forebody geometry can be held fixed. To simplify the problem, a series of two-dimensional flat ramps, comparable to a typical two-dimensional inlet, is used to initially compress the flow. For the present work, the flow is compressed by three flat ramps, the first ramp inclined at 5 deg and the second and third ramps inclined at 4 deg. The flow is turned a total of 13 deg before entering the transition. The actual computational solution begins at the cowl lip, as shown in Fig. 1

Design Variable Formulation

The goal in choosing the proper geometric parameters for this optimization was to limit the number of variables, reducing the total runtime of the optimization, while keeping the geometry flexible enough to produce the desired result. A Bezier–Bernstein curve is used to reduce the number of design variables, as suggested by Burgreen et al.[8] Such a curve allows for the top compression centerline to have a fairly complex shape, yet requires less design variables than would be necessary with other formulation. The top compression centerline is defined by a two-dimensional fifth-order Bezier–Bernstein curve. This centerline determines the two-dimensional properties of the inlet. Cancellation of the shock eminating from the cowl lip is one of the more important aspects of the optimization, and, therefore, this shape is allowed to vary as much as possible within the optimizer.

The slope of the curve at the beginning of the transition duct is held fixed to maintain continuity with the forebody compression ramps. The slope of the curve at the expansion corner is allowed to vary, allowing for the possibility of a small sharp corner at the entrance to the combustion chamber. The distance between the cowl lip plane and the expansion corner plane is also allowed to vary, thus changing the position of this corner. This leaves six coordinates for Bezier–Bernstein control points, X_2, X_3, Y_3, X_4, Y_4, and X_5, which are allowed to vary within the optimization. This curve determines the shape of the centerline of the top surface of the transition duct.

The shapes of the cross sections are determined by averaging the desired capture cross section with the desired combustor cross section. In the present work, a hyperellipse, defined by the equation $x^n + y^n = 1$, is used instead of a rectangle for prescribing the capture cross section. Experience showed that a reasonable value of n is 20, which results in a less than 1% loss in mass flow capture compared

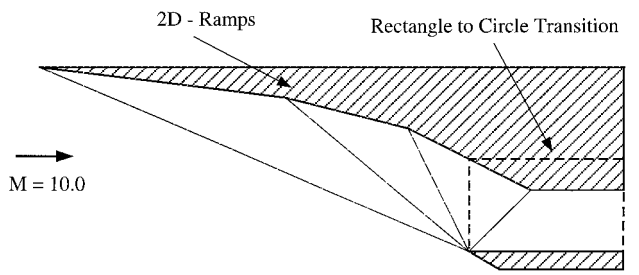

Fig. 1 Location of the computational zone for rectangular-to-circular transition with uniform inflow.

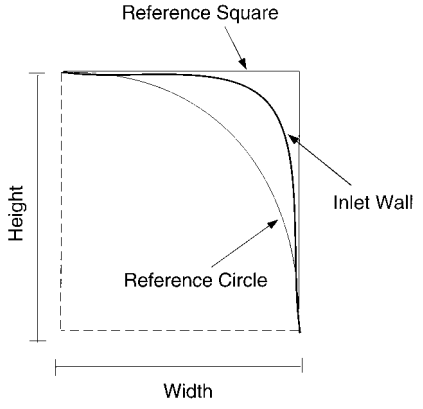

Fig. 2 Geometric parameters defining the shape of an intermediate cross section.

to an infinitely sharp corner. The benefit of using the hyperellipse is that it allows for a more stable computational solution, which is necessary for use with an optimizer. The hyperellipse is then scaled by the desired dimensions of the capture plane. Separate scaling factors are used for both the top and bottom portions of the inlet.

For the intermediate planes, the cross-sectional shape is averaged using a fractional value. Two fractional values, Δ_u and Δ_l, are included as design variables for six intermediate planes that are allowed to change during the optimization process. The fractional values between the prescribed planes are interpolated using cubic splines. Each fractional value is a weight that is applied to an averaging of the hyperellipse and a circle. The radius for a given angle is determined for the intermediate plane by the following equation:

$$(1 - \Delta_x)(R_{\text{hyperellipse}}) + \Delta_x(R_{\text{circle}}) = R_{\text{final}} \tag{1}$$

A separate value of Δ is used for both the top quarter and the bottom quarter of the intermediate plane. The intermediate shape is determined by Eq. (1). The shape is then scaled by the height of the plane, determined by the Bezier–Bernstein curve and by the width of the plane, which is held fixed through the transition. The value of Δ is held fixed to zero at the capture plane and one at the combustor plane. An example of this averaging is shown in Fig. 2.

For the present optimization, certain aspects of the transition geometry are held fixed. The height of the capture planes is set to 2.9 times the diameter of the combustor and is fixed such that all three forebody shock waves intersect at the cowl lip for maximum mass capture. With the 6 design variables allocated for the Bezier–Bernstein curve, and a total of 12 variables to determine the cross-sectional shape, this allows for a total of 18 design parameters that can vary during the optimization.

Objective Function Formulation

The key to obtaining the desired combustor flow properties in the proper choice of an objective function to be minimized or maximized. For this work, an area-averaged standard deviation of the pressure is chosen as the objective function, to maximize flow uniformity. For each plane, an average pressure is calculated based on the area,

$$\bar{P} = \Sigma\, P_i A_i / \Sigma\, A_i \tag{2}$$

This area averaged pressure is then used to calculate a modified standard deviation of the pressure:

$$\sigma_P = \sqrt{\frac{\Sigma\, A_i (P_i - \bar{P})^2}{\Sigma\, A_i}} \tag{3}$$

This calculation is then repeated over three planes between the expansion corner and the exit, with each of these values averaged. This ensures that the optimizer will not converge to a local minimum in which a shock wave reflects off of a wall exactly at the plane where the standard deviation is calculated. When the objective is extended into the combuster, the overall effect of the optimization should be to minimize the expansion and compression waves that continue into the combustor.

Design Conditions

The design conditions chosen for this optimization were for a Hyper-X class vehicle flying on-design, at a cruise Mach number of 10. The inlet was chosen to provide an overall static pressure rise of 100 times the freestream value into the combustor. A 5-deg forebody compression ramp is followed by two 4-deg forebody compression ramps, providing an overall pressure ratio of $P_{\text{fore}} = 12.8$. This requires the pressure ratio for the transition to be $P_{\text{trans}} = 7.8$, which is reasonable given the geometric constraints chosen for this study. The freestream Mach number was set to $M_\infty = 10$, and, as such, the capture plane properties were set to the conditions after the freestream flow had been compressed by the three forebody compression ramps. The inflow Mach number to the transition was determined to be $M_{\text{cap}} = 6.54$.

Uniform Inflow Optimization Results

For the run shown in Fig. 3, the optimal design was determined after a total of 291 function evaluations, of which 234 function evaluations were used to determine gradients, and 57 function evaluations were used to reduce the objective function. A total of 170 CPU h were required to obtain the optimized solution. The initial design point produced an inlet with a 20.3% standard deviation in pressure across the combustor plane. The final solution produced by the optimizer reduced this value to 7.7%. The function evaluation history over the optimization is shown in Fig. 3.

An attempt was made to reduce the value of σ_P further, with the same number of grid cells for the computational solution; however, for all optimization runs attempted, the optimizer was unable to proceed any further. The finite differenced gradients calculated by the optimizer are reduced in accuracy as the algorithm proceeds to the optimum solution, which would theoretically be a 0% standard deviation in pressure. The only way to obtain a better solution would be to increase the number of grid points used for the computational solution, thereby increasing the accuracy of the gradient calculations. However, as with all three-dimensional computational fluid dynamics problems, adding grid points can dramatically increase the required CPU time. With the given code, if the number of points in the i, j, and k directions are doubled, the required CPU time will typically increase by a factor of eight. Thus, the additional accuracy gained might not justify the additional computational effort. The goal is to allow the solution to have enough accuracy to obtain a usable design in a reasonable amount of time.

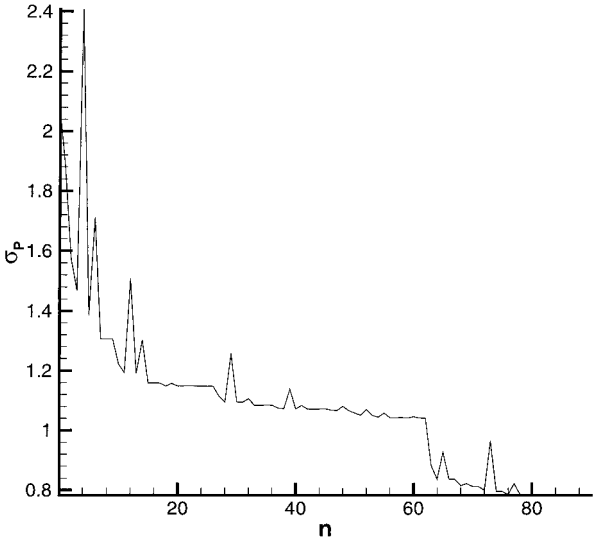

Fig. 3 Optimization function evaluation history for uniform inflow.

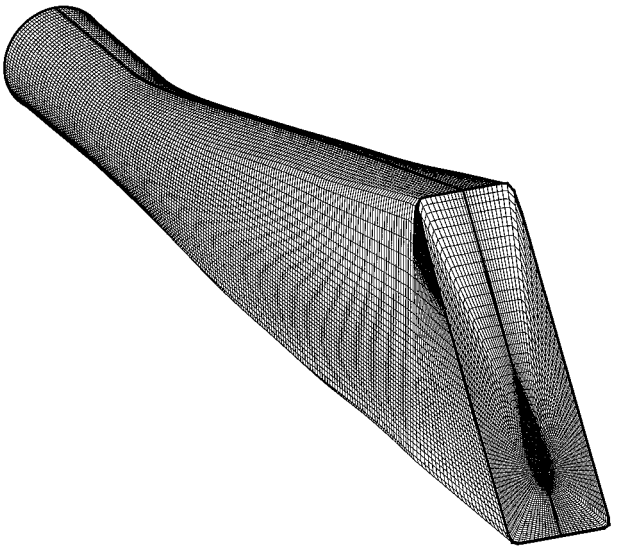

Fig. 4 Mach 10 optimized inlet with uniform inflow.

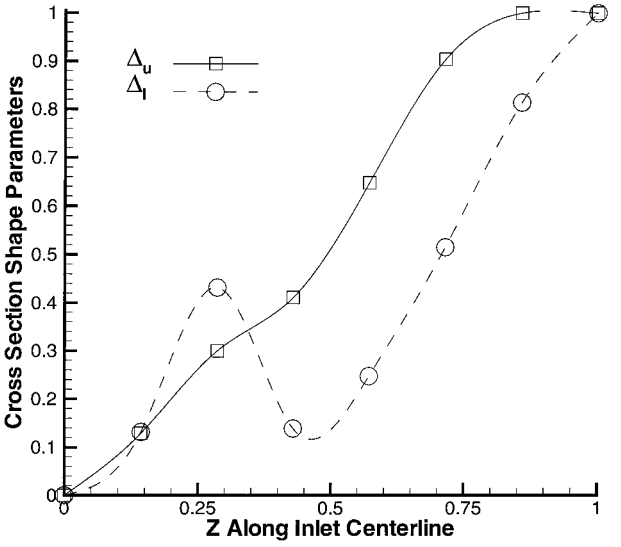

Fig. 5 Cross-sectional shape percentages along Mach 10 optimized inlet with uniform inflow.

The final optimized configuration is shown in Fig. 4. The transition section length was found to be 8.4 times the diameter of the combustor cross section. An interesting aspect of this optimal shape is the manner in which the cross-sectional shape varies along the transition duct. The final values of Δ_u and Δ_l along the transition are shown in Fig. 5. The values for the upper portion of the inlet behave monotonically, with the cross-sectional shape becoming completely circular just before the end of the transition duct. The lower values, however, vary greatly. The lower portion transitions to a circle more quickly than the upper section, initially; it then returns to a more rectangular shape and then quickly transitions back to the circular shape. This has the effect of creating a shallow compression at this lower corner, followed by a sharper expansion, then another compression. This shape can be seen in Fig. 4 as a small dent at the lower corner, toward the front of the transition duct. This property appeared in several preliminary runs and appears to be necessary to cancel compression waves originating from the upper corner.

Most of the Bezier–Bernstein curve control points did not vary greatly through the optimization. The most important parameters appear to be the length of the transition duct and the control points that determined the angle at which the transition piece centerline terminated. Each of these values varied from 5–10%, whereas the other parameters varied by less than 1% over the entire optimization.

Table 1 Grid dependence comparison of pressure deviation and total pressure parameters for uniform flow design

	Optimized		Nonoptimized	
Parameter	Coarse[a]	Fine[b]	Coarse[a]	Fine[b]
σ_P,%	9.94	9.72	12.92	13.41
$\bar{P}$	7.976	8.019	7.984	8.014

[a]Coarse grid is $60 \times 40 \times 166$. [b]Fine grid is $120 \times 80 \times 332$.

Fig. 6 Pressure contours on walls of optimized uniform inflow inlet at on-design conditions.

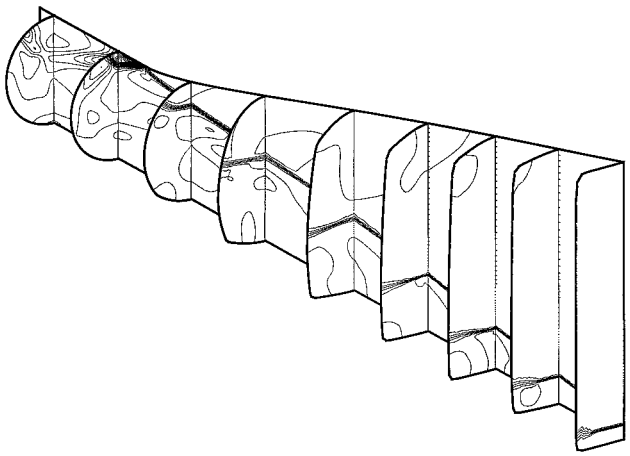

Fig. 7 Pressure contours inside optimized uniform inflow inlet at on-design conditions.

The pressure contours both along the walls and inside the transition duct are shown in Figs. 6 and 7, respectively. As can be seen, there appear to be fairly strong compression waves present near the expansion corner. These waves are followed by a strong expansion wave, originative from the corner, which quickly cancels out this compression and brings flow to relatively uniform pressure toward the combustor entrance plane. Areas of higher pressure occur along the combustor planes and are spread over 4–6 grid cells. These sharp rises in pressure, about 20% higher than the average pressure at this plane and occurring over a small number of grid cells, are difficult for the optimizer to remove completely. However, the remainder of the combustor plane is fairly uniform in pressure.

Grid Dependence

A grid-dependence study was conducted to assess the accuracy of the objective function [Eq. (3)] over the course of the optimization. The number of points in each of the compuational directions was doubled, and the objective function was calculated. These calculations were made for two geometries: a geometry close to the optimum solution and a geometry far from the optimum solution. The results of this study are shown in Table 1.

For the starting geometry, the area-averaged standard deviation in pressure across the combustor planes was 4% less for the coarse grid than for the fine grid. As the solution progressed to the optimum, this difference was reduced to 1.8%. Apparently, as the solution progresses toward providing uniform flow to the combustor, the flowfield gradients decrease as reflected shock waves and expansion waves are removed from the solution. With this reduction in complexity, fewer grid points are necessary to obtain a reliable solution. As this study shows, it is apparent that the number of grid points chosen provides sufficient accuracy for use with the optimizer.

Nonuniform Inflow Optimization

To simplify the problem, one inversely designed compression surface is allowed to vary during the overall optimization, with two other compression surfaces held as fixed geometries. A 5-deg two-dimensional ramp followed by a 4-deg two-dimensional ramp are used to initially compress the flow. An inversely designed power-law ramp is then used to provide the nonuniform inflow conditions to the transition duct. The actual computational solution for the optimizer begins at the cowl lip, as shown in Fig. 8.

Forebody Generation

The stream-traced power-law section of the compression forebody is derived using inverse-design techniques developed for the determination of waverider geometries.[3] Normally, these shapes are derived from basic flowfields that are analytically determined, such as wedge flows or conical flows. For the present work, the flowfield over a two-dimensional three-fourths power-law geometry was chosen. This geometry offers the optimizer a nonuniform flowfield with the pressure varying by up to 30% across the inlet capture plane. The amount of nonuniformity is important because the goal of this part of the study is to investigate the impact of a nonuniform flowfield on the results of the optimization process, as well as the overall inlet performance.

The actual shape of the ramp is determined by choosing a point in the flowfield and numerically tracing the streamline backward to its intersection with the shock. The flow between this streamline and the shock determines the inflow conditions to the inlet transition duct.

Compression Surface Definition

The actual stream-traced compression surface is determined using a technique similar to that used by Sabean and Lewis[9] in the design of a power-law derived star body. In the case of the present work, one streamline is chosen to represent the two-dimensional compression ramp. This streamline is determined by using two variables to determine a point in the flow that will correspond to the top of the rectangular-to-circular transition duct capture plane. The streamline corresponding with this point is then traced backward until it intersects with the shock wave, thus determining the compression surface. The flow between this point and the shock wave represents the flow entering the transition duct. A diagram of this configuration is shown in Fig. 9. The line representing the transition duct capture plane is shown inclined at 9 deg because the flow over this compression surface has already been turned a total of 9 deg by the two initial flat compression ramps. The properties along this line are

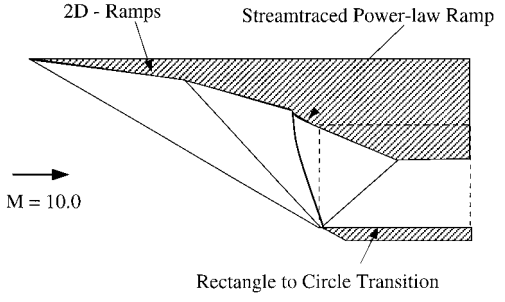

Fig. 8 Location of the computational zone for rectangular-to-circular transition with nonuniform inflow.

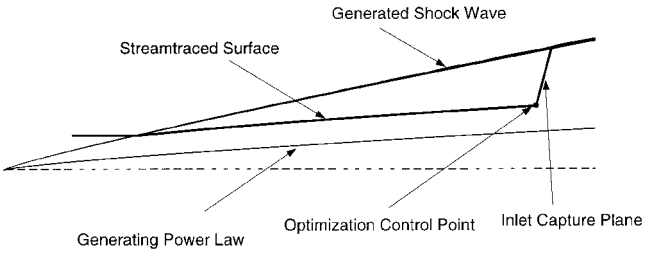

Fig. 9 Determination of streamtrace power-law compression surface and inflow conditions.

then scaled according to the fixed height of the capture plane and are used as inputs to the transition duct flow solver.

Power-Law Flowfield Computational Scheme

GASP[5] is used to generate the flowfield used in the inverse-design process. This finite volume code is used to solve the two-dimensional Euler equations over a power-law shape with the form $y = Cx^{3/4}$. The value of C was adjusted along with the internal contraction ratio of the inlet to produce an overall compression ratio of 100 for the entire forebody and inlet. In this case, the value of C corresponded to a power law with a length of 1.0 and a height of 0.094. The actual values of x and y are scaled so that the desired capture area flowfield would fit within the actual inlet capture area.

The grid is generated algebraically using this same functional form, with clustering near $x = 0$ to better capture the flow properties at the nose. The grid is also broken into two zones: a subsonic zone with 90×102 grid points and a supersonic zone with 112×140 grid points. The calculations in the supersonic zone are done using space marching to lower the overall runtime required per calculation. As such, a complete calculation requires 80 CPU min on a DEC Alpha 433.

The flow is calculated in the subsonic region using Van Leer flux vector splitting with a min–mod limiter and is globally iterated using a two-factor approximate factorization method. The supersonic region uses a full flux in the marching direction, with a catastrophic limiter based on the pressure and density of the flow in the transverse direction, as well as a first-order-accurate LU decomposition on a single line with relaxation in the sweep direction. Inviscid wall boundary conditions are used because the final body surfaces are taken from stream surfaces that do not coincide with the generating surface. The flow is assumed to be nonreacting air with a constant value of $\gamma = 1.4$ and an initial Mach number of 7.31 corresponding to a Mach 10 freestream flow that has passed over a 5-deg wedge, followed by a 4-deg wedge.

Design Variable Formulation

The design variables used to describe the geometry of the power-law inlet are identical to those used for the uniform inflow case. Two additional design variables are added to determine the inverse design compression surface. As was the case for the preceding optimization problem, certain aspects of the geometry were held fixed. The height of the capture plane is set to 2.3 times the diameter of the combustor and is fixed such that all three forebody shock waves intersect at the cowl lip for maximum mass capture. With the 2 design variables used to determine the inversely designed inflow conditions, 6 design variables allocated for the Bezier–Bernstein curve, and a total of 12 variables to determine the cross-sectional shape, there are a total of 20 design parameters that can vary during the optimization.

Objective Function Formulation

The same area-averaged standard deviation in pressure given in Eq. (3) is used for the objective function for the nonuniform inflow optimization.

Design Conditions

The same flight conditions were used to determine the nonuniform inflow geometry. A 5-deg forebody compression ramp is followed by

a 4-deg forebody compression ramp, providing an overall pressure ratio of $P_{\text{fore}} = 6.49$ for the fixed compression ramps. This requires that the pressure ratio for the stream-traced compression surface and the transition duct to be $P_{\text{stcomp}+\text{trans}} = 15.4$, which is reasonable for the geometric constraints chosen for this study. The freestream Mach number was set to $M_\infty = 10$, and, as such, the capture plane properties were set to the conditions after the freestream flow had been compressed by the three forebody compression ramps, as determined by the inverse-design flowfield.

Nonuniform Inflow Optimization Results

For the run shown in Fig. 10, the optimal design was determined after a total of 551 function evaluations, of which 447 function evaluations were used to determine gradients, and 104 function evaluations were used to reduce the objective function. A total of 321 CPU h were required to obtain the optimized solution. The initial design point produced an inlet with a 16.9% standard deviation in pressure across the combustor plane. The final solution produced by the optimizer reduced this value to 9.9%. The function evaluation history over the optimization is shown in Fig. 10. As was done with the uniform inflow optimization, an attempt was made to reduce the value of σ_P further, with the same number of grid cells for the computational solution; however, for all optimization runs attempted, the optimizer was unable to proceed any further.

The final optimized configuration is shown in Fig. 11. The transition section length was found to be 7.88 times the diameter of the

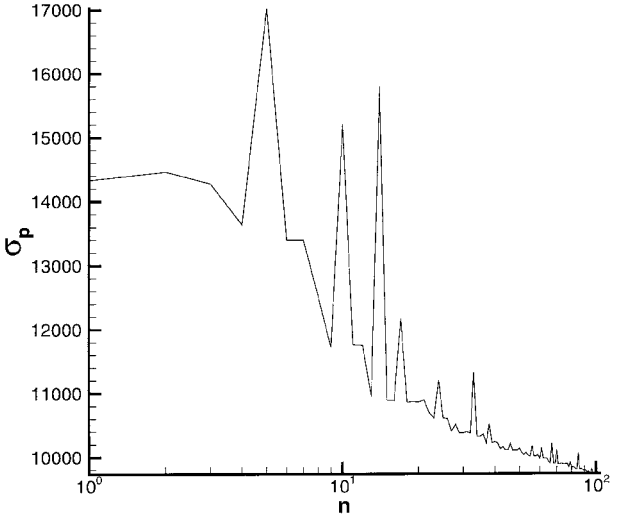

Fig. 10 Optimization function evaluation history for nonuniform inflow.

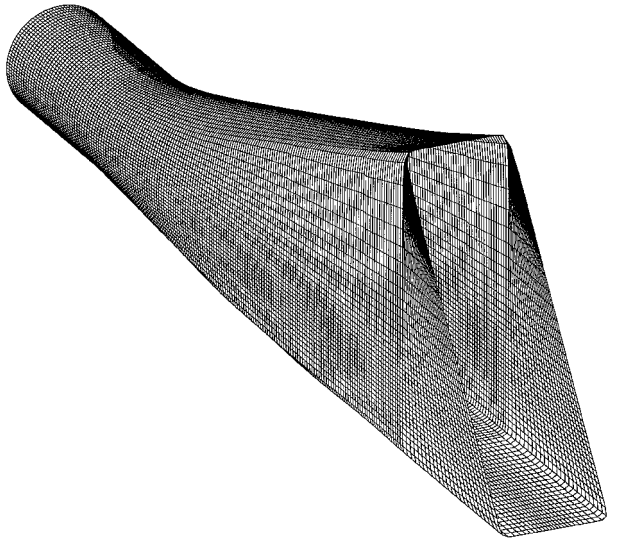

Fig. 11 Mach 10 optimized inlet with nonuniform inflow.

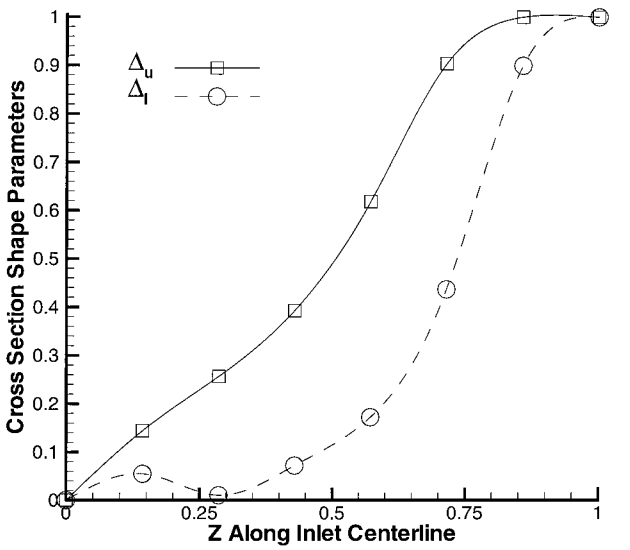

Fig. 12 Cross-sectional shape percentages along Mach 10 optimized nonuniform inflow inlet.

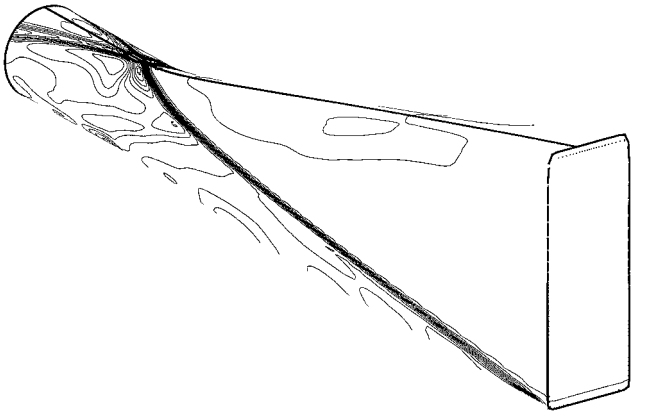

Fig. 13 Pressure contours on walls of optimized nonuniform inflow inlet.

combustor cross section. An interesting aspect of this optimal shape is the manner in which the cross-sectional shape varies along the transition duct. The final values of Δ_u and Δ_l along the transition are shown in Fig. 12. The values for the upper portion of the inlet behave monotonically, much the same as with the uniform inflow case; however, the lower values behave quite differently. The indentation that occurs with the uniform inflow optimization is again present in the nonuniform inflow optimization; however, the indentation is much less pronounced.

Another major difference between the two optimization cases is that the shape of the Bezier–Bernstein curve varies greatly throughout the nonuniform inflow optimization. The inlet centerline curvature must match that of the power-law stream-traced ramp, otherwise additional unwanted expansion and compression waves will be produced. The X and Y values of the Bezier–Bernstein control points varied 2–10% over the course of the optimization. As such, it was found that careful selection of all of the design variables was integral to the successful completion of the optimization.

The pressure contours both along the walls and inside the optimal transition duct are shown in Figs. 13 and 14, respectively. As can be seen, there appear to be fairly strong compression waves present near the expansion corner. These waves are followed by a strong expansion wave, originating from the corner, which quickly cancels out this compression and brings the flow to relatively uniform pressure toward the combustor entrance plane. Again, areas of high pressure occur over small regions along the combustor plane, as occurred for the preceding optimization. Because these peaks occur over a small area, their impact on the objective function is averaged out, making

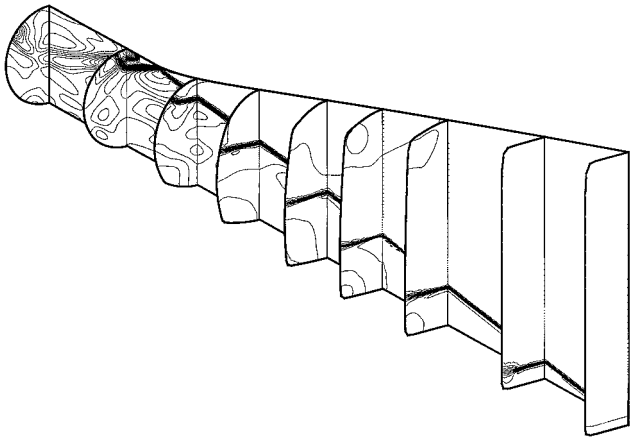

Fig. 14 Pressure contours inside optimized nonuniform inflow inlet.

it difficult for the optimizer to remove them completely. A choice of an objective function that accurately represents the effects of these peaks would be necessary to remove them.

Inlet Performance

To determine the benefits of the optimized configurations, the performance is compared to a corresponding two-dimensional inlet designed for the same conditions.[10] To obtain an overall compression ratio of 100, a system of three compression ramps is again used; however, all three ramps are inclined at 5 deg, for an overall turning angle of 15 deg. In conjunction with a square combustor, this configuration will produce approximately the same compression ratio as the optimized rectangular-to-circular configuration presented earlier.

Three commonly used efficiency parameters,[11] total pressure recovery π_c, adiabatic compression efficiency η_c, and kinetic energy efficiency η_{ke} are calculated and mass flow averaged over the combustor plane. Each of these values for the optimized power-law stream-traced inlet case, over several Mach numbers, are shown in Table 2. These values can be directly compared to those for the optimized uniform capture inlet case, shown in Table 3. The values for both inlets can be compared to the values for a two-dimensional inlet, which are shown in Table 4. As can be seen, the rectangular-to-circular transition duct is more efficient than the two-dimensional case. This is mainly due to the extra compression received from the transitioning of the corners to the circular shape. However, the stream-traced power-law inlet does not perform as well as the other two cases. This is to be expected because the power-law compression surface is not as efficient as a simple flat compression surface. However, at a small performance cost at the inlet, a nonuniform inversely designed forebody can be included in the vehicle design and then corrected to provide uniform flow to the combustor.

Note that these efficiencies were determined using inviscid calculations. The presence of interactions between the turbulent boundary layer and shock waves present in the flow can have a significant impact on the flow uniformity and inlet efficiency. As such, these values should be viewed as an upper limit on the efficiency parameters. An analysis of these interactions could be incorporated into the optimizer, to minimize the impact on the overall inlet efficiency, though this has been left for future work.

Viscous Considerations

All of the numerical calculations of the transition duct flowfield in the present work were done assuming the flow was inviscid; however, as noted, the presence of a boundary layer could have adverse effects on the overall performance of the inlet. For instance, these inviscid solutions do not take into account the three-dimensional shock/boundary-layer interactions that can possibly occur. Work by Korkegi[6] presents a correlation for predicting the occurrence of two classes of such interactions:

Table 2 Inlet efficiencies for optimized rectangular-to-circular inlets with power-law compression, as a function of design Mach number

Efficiency	Mach 6.0	Mach 8.0	Mach 10.0
π_c	0.689	0.543	0.413
η_c	0.949	0.934	0.924
η_{ke}	0.984	0.985	0.985

Table 3 Inlet efficiencies for optimized rectangular-to-circular inlets with uniform capture, as a function of design Mach number

Efficiency	Mach 6.0	Mach 8.0	Mach 10.0
π_c	0.736	0.614	0.489
η_c	0.958	0.946	0.937
η_{ke}	0.987	0.988	0.988

Table 4 Inlet efficiencies for two-dimensional inlets, as a function of design Mach number

Efficiency	Mach 6.0	Mach 8.0	Mach 10.0
π_c	0.716	0.560	0.427
η_c	0.944	0.934	0.929
η_{ke}	0.986	0.986	0.986

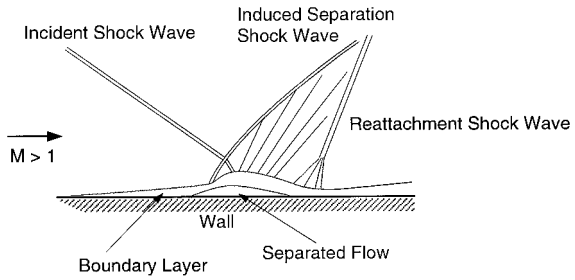

Fig. 15 Two-dimensional shock wave intersecting a turbulent boundary layer.

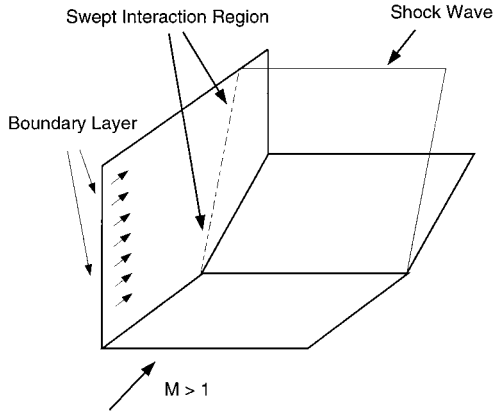

Fig. 16 Skewed shock wave intersecting a turbulent boundary layer along a side wall.

1) Case 1 involves incipient separation due to a two-dimensional shock wave intersecting a turbulent boundary layer as shown in Fig. 15.

2) Case 2 involves incipient separation due to a skewed shock wave intersecting a turbulent boundary layer along a side wall as shown in Fig. 16.

To determine where separation could possibly occur in the present designs, a method suggested by Smart[1] is used. Each of the two possible separation cases is unique, and, as such, it should be possible to address each of the separation criteria individually. Streamline

traces were generated along the surface of the final inlet configurations. Korkegi's correlations were then applied over each of these streamlines, after an appropriate transformation to the streamline coordinate system. For both of the optimized configurations, Korkegi's correlations show that separation due to case 1 does not occur in this inlet configuration, most notably at the intersection of the reflected shock with the expansion corner. Conditions for case 2, however, do occur over the intersection of the shock with the top corners of the rectangular-to-circular transition. This means that although the problem of hypersonic corner flow has been removed from the configuration, a new problem of separation has been introduced. The severity of these interactions should be explored more thoroughly before this inlet design could be used in an actual flight application.

Conclusions and Future Work

The optimizations performed produced designs that decreased the area-averaged standard deviation in pressure across the combustor plane to 9.9%. A lower value may be possible with increased CPU time required, though this may not necessarily be worth the increase in uniformity. It might also be possible to employ a different objective function that would not decrease substantially in accuracy as the optimal solution was approached.

The results for the uniform inflow optimization are similar to those in the work of Smart,[1] who found that rectangular-to-elliptical transition geometries tend to outperform two-dimensional inlets at the same design point. This is most likely due to the additional compression that occurs as the corners of the rectangle transition into smoother elliptical shapes. For the case of such a transition that utilizes a stream-traced power-law compression surface, the inlet is less efficient. This result is not surprising; the compression surface was chosen to demonstrate the capability of optimizing such a transition with a nonuniform capture flowfield. The power-law flowfield allows for this, though it is much less efficient at compressing the flow than a flat ramp. Thus, the efficiency of the inlet is sacrificed by using this particular inverse-design forebody.

The strength of the nonuniform inflow design technique is that the shape of the transition duct can be adjusted to compensate for using a flowfield with a 10–20% change in pressure across the capture plane to produce a more uniform flow into the combustor. In previous studies involving the use of inversely designed shapes for the design of airframe-integrated scramjets, there has been concern that the use of a nonuniform flowfield for the generation of the forebody would have adverse affects on the uniformity of the flow delivered to the combustor.[3] Other methods of inverse-design forebody generation have been used to attempt to provide more uniform flow to the inlet while maintaining the high L/D properties, including the so-called waverider shapes.[11] However, a forebody that produces uniform flow will not deliver uniform flow to a cylindrical combustor without the development of a three-dimensional design. The present study demonstrates that the problem of delivering uniform flow to the combustor can be effectively decoupled from the choice of the initial forebody compression surface, within reason. Ideally, a forebody derived using traditional inverse-design flowfields could be coupled with an optimization similar to that presented here to obtain both high L/D as well as a more efficient inlet.

These optimization procedures can also be applied to the design of an inlet for minimum viscous drag. Using a small crossflow boundary-layer assumption, as done by Smart,[1] an approximate boundary layer could be calculated using the inviscid computational solution. This boundary-layer calculation could then be used to approximate the total viscous drag acting on the inlet, which could then be used as the objective function for the optimizer, with flow uniformity included as a constraint to the optimizer.

Note that in addition to viscous drag losses, complex three-dimensional shock wave/turbulent boundary-layer interactions can also occur inside the transition duct. Smart[1] has addressed these interactions and has used a combination of separation correlations by Korkegi[6] to predict whether any such interactions occur inside the REST inlet. This same method could be adopted into the numerical optimizer as a constraint, though this is left for future work.

Overall, a numerical optimization routine coupled with a computational flow solver can produce a rectangular-to-circular transition duct with adequately uniform flow, even when the flow at the entrance to the duct is not necessarily uniform. The transition duct is not as efficient as its two-dimensional counterpart; however, this may be an acceptable design tradeoff, depending on the desired application.

Acknowledgments

This work was supported by NASA Grant NGT 52158, Charles Cockrell, Jr. Technical Monitor, to whom appreciation is expressed. Thanks also go to Lloyd Evans from the NASA Langley Research Center Education office for support of this work. Appreciation is also expressed to Michael Smart for his technical input.

References

[1] Smart, M., "Design of Three-Dimensional Hypersonic Inlets with Rectangular to Elliptical Shape Transition," AIAA Paper 98-0960, Jan. 1998.

[2] Shukla, V., Gelsey, A., Schwabacher, M., Smith, D., and Knight, D., "Automated Redesign of the NASA P8 Hypersonic Inlet Using Numerical Optimization," AIAA Paper 96-2549, July 1996.

[3] O'Neill, M., and Lewis, M., "Optimized Scramjet Integration on a Waverider," *Journal of Aircraft*, Vol. 29, No. 6, 1992, pp. 1114–1121.

[4] McClinton, C., Voland, R., Holland, S., and Engelund, W., "Wind-Tunnel Testing, Flight Scaling, and Flight Validation with Hyper-X," AIAA Paper 98-2866, April 1998.

[5] GASP, Ver. 3.0, Aerosoft, Inc., Blacksburg, VA, 1996.

[6] Korkegi, R., "Comparison of Shock-Induced Two- and Three-Dimensional Incipient Turbulent Separation," *AIAA Journal*, Vol. 13, No. 4, 1975, pp. 534, 535.

[7] *DOT User Manual, Version 4.00*, VMA Engineering, Goleta, CA, 1993.

[8] Burgreen, G., Baysal, O., and Eleshaky, M., "Improving the Efficiency of Aerodynamic Shape Optimization," *AIAA Journal*, Vol. 32, No. 1, 1994, pp. 69–76.

[9] Sabean, J., Lewis, M. J., Mee, D., and Paull, A., "Performance Study of a Power Law Star Body," *Journal of Spacecraft and Rockets*, Vol. 36, No. 5, 1999, pp. 646–652.

[10] Takashima, N., and Lewis, M., "Engine–Airframe Integration on Osculating Cone Waverider-Based Vehicle Designs," AIAA Paper 96-2551, July 1996.

[11] Heiser, W., and Pratt, D., *Hypersonic Airbreathing Propulsion*, AIAA Education Series, AIAA, Washington, DC, 1994, pp. 204–208.